Nanotechnology and Regenerative Medicine

A Novel Method Using Quantum Dots for Testing the Barrier Function of Cultured Epithelial Cell Sheets

Thomas J. Duncan,[1] Koichi Baba,[2] Yoshinori Oie,[1] and Kohji Nishida[1]

[1]Department of Ophthalmology, Osaka University Graduate School of Medicine, Suita, Japan
[2]Department of Visual Regenerative Medicine, Osaka University Graduate School of Medicine, Suita, Japan

PURPOSE. The corneal epithelium provides a barrier to protect the deeper structures of the eye from any particles or pathogens. Cultured epithelial cell sheets are used in transplantation surgery for corneal repair or regeneration. The purpose of this study was to develop a novel method using fluorescent quantum dot nanoparticles for validating the quality and barrier function of cultured epithelial cell sheets.

METHODS. Human function epithelial cell sheets, cultured from oral mucosal or corneal limbal cells, were incubated in either normal calcium-containing medium or medium containing no calcium with a calcium chelator. Also contained in the media were suspensions of two different sizes of quantum dots. Following incubation, analysis of quantum dot penetration was carried out using confocal microscopy.

RESULTS. In contrast to the cell sheets incubated in calcium-containing medium, removal of extracellular calcium resulted in the disruption of tight junctions, compromising the cell sheet's barrier function. This caused a reduction in transepithelial electrical resistance and deeper, more ubiquitous penetration of the quantum dots into the paracellular space and interior of the cell sheet.

CONCLUSIONS. This method provides easy to interpret qualitative and quantitative data on the functionality of a cell sheet's tight junctions, as well as nanoscale and microscale structural information on its surface and interior morphology, and any localized areas of damage or abnormality. This novel technique could be used as part of the validation system for cultured epithelial cell sheets for use in transplantation.

Keywords: tight junction, quantum dots, epithelial cells, barrier function

Anteriorly, the ocular surface is covered by specialized corneal, limbal, and conjunctival epithelia. The corneal epithelium is characterized by stratified, squamous, nonkeratinized epithelial cells that are responsible for maintaining the smooth refractive surface of the cornea, essential for vision, while also acting as a protective barrier to prevent the passage of foreign bodies and pathogens into the deeper ocular structures. Corneal epithelial cells are derived from transient amplifying cells generated by stem cell populations residing in the basal layer of the limbal epithelium.[1,2] Ocular disease or trauma to this area such as Stevens-Johnson syndrome, thermal or chemical burns can cause limbal stem cell deficiencies that result in corneal invasion by adjacent conjunctival cells, neovascularization, chronic inflammation, and stromal scarring. Consequently, visual acuity is severely affected.[3,4] In cases of unilateral damage, corneal regeneration of the affected ocular surface can be attempted by transplantation of limbal grafts[5] or via the cultivation of epithelial cell sheets from autologous limbal stem cells taken from the contralateral eye.[6–8] However, this requires a large limbal graft from the donor eye, carrying with it a risk of infection and inducing a limbal stem cell deficiency in the donor eye.[9] It is also unsuitable for patients who have bilateral corneal damage.[10] Transplantation from allogenic donors necessitates prolonged use of postoperative immunosuppressants,[11] and carries a high risk of rejection. Postoperative rates of rejection after 1-year range from 20% to 60% with cadaveric donor tissue,[5,12] and 70% to 80% with living donor tissue.[13,14]

In an attempt to improve postsurgical results for corneal surface reconstruction, recent studies have successfully fabricated and transplanted epithelial cell sheets cultured ex vivo from autologous epithelium of nonocular surface origin.[15,16] In rabbits, the technique for harvesting, culturing, and transplanting autologous oral mucosal epithelial cell derived cell sheets has been established.[17,18] More recently, the same treatment has been subjected to clinical trials in humans.[19,20] A 14-month postoperative evaluation showed significantly improved visual acuity was maintained and no complications were observed, with the oral mucosal keratinocytes undergoing phenotypic changes to more closely resemble that of corneal keratinocytes.[19] Before this emerging technique can become a standard medical therapy however, it is crucial to establish a validation system by which the cultured oral mucosal epithelial cell sheets can be evaluated prior to transplantation. Such a validation system has been outlined in a previous study by Hayashi et al.[21]

One such parameter for evaluation is a cell sheet's barrier function, a measure by which it can control or inhibit the passage of molecules, foreign bodies or pathogens across its cell layers. The tight junction is the most apically located of the junctional complexes, forming a continuous, belt-like structure that seals the paracellular pathway by joining the lateral surfaces of the most superficial layer of epithelial cells at their

2215

Investigative Ophthalmology & Visual Science

apical edge.[22,23] Calcium has been shown to be necessary for establishing the paracellular connections and assembly of the various proteins involved in a tight junction complex.[24–27] Removal of calcium, through the use of a calcium chelator, disrupts tight junction structure and function.[24,25,28] Evaluating the barrier function and health of the tight junctions in a cultured epithelial cell sheet is necessary prior to its use in transplantation surgery.

Transepithelial electrical resistance (TEER) is a technique that measures the electrical resistance across the full thickness of the cell sheet using two electrodes placed above and below. Primarily, this technique is used to obtain information on the barrier function of a cell sheet. However, TEER values are often unreliable. Numerous studies have reported that TEER does not accurately represent changes in tight junction structure or function.[29,30] Furthermore, the overall electrical resistance of a cell sheet has been shown to be significantly affected by other factors including temperature,[31] the culture substrate used,[32] and the degree of cell-substrate contact.[33]

Quantum dots are nanometer scale colloidal semiconductor nanoparticles composed of a few hundred to a few thousand atoms of a semiconductor material such as cadmium mixed with tellurium or selenium. This is then coated with an additional zinc sulfide semiconductor shell to contain the cadmium and limit its dissolution, as well as improve the quantum dot optical properties.[34] Bioconjugation of this shell to proteins or other small molecules serves to further enhance their biological applications. Quantum dots are extremely efficient at generating fluorescence, often many times greater than that of conventional organic fluorescent compounds.[34,35] They have a board excitation spectra with a narrow emission spectra ranging from UV to near-infrared, and superior photostability with a high resistance to photo-bleaching, allowing for greater observation time or long-term imaging experiments.[36-38] One highly advantageous property of quantum dots is that their fluorescence is tunable. A predictable relationship exists between the energy emitted by these quantum dots (and consequently the wavelength of their fluorescence) and the size and shape of the quantum dot core, with smaller quantum dots fluorescing at shorter wavelengths of light than larger quantum dots. Applying quantum dots to the surface of bovine cornea in vitro has shown that penetration is limited to only the superficial epithelial layers, 20 μm from the corneal surface.[39] In this healthy cornea, the epithelium acted as a barrier to limit quantum dot penetration. Quantum dots may therefore represent a suitable candidate for evaluating the barrier function of a cell sheet.

The purpose of this study is to use these nanoparticles to provide qualitative and quantitative data specific to a cell sheet's morphology and tight junction functionality. We hypothesize that cell sheets with damaged or disrupted barrier function will permit deeper and more ubiquitous penetration of the quantum dot nanoparticles. Additionally, by using different sized quantum dots, we anticipate a size-dependent variation in penetration and distribution.

METHODS

Cell Culture: Human Oral Mucosal Epithelial Cell Sheets

Human oral mucosal keratinocytes (HOK; ScienCell Research Lab, Carlsbad, CA, USA) were cultured until subconfluent. Trypsin LE express (GIBCO Invitrogen Life Technologies, Grand Island, NY, USA) was used to detach the cells from the culture flask into suspension. The cell suspension was then centrifuged and the supernatant removed. The cells were then resuspended in keratinocyte culture medium and seeded at an initial cell density of 1×10^5 cells/mL into 12-well culture inserts (Falcon, Corning, NY, USA) with mitomycin C (MMC)-treated 3T3-J2 feeder cells in keratinocyte culture medium (KCM), separated by the cell culture insert permeable membrane. KCM comprises Dulbecco's modified Eagle's medium (DMEM/F12 [3:1]) supplemented with 10% fetal bovine serum (GIBCO Invitrogen Life Technologies), 1% L-Glutamine (GIBCO Invitrogen Life Technologies), 5 μg/mL insulin (novolin; Novartis Pharmaceuticals, Tokyo, Japan), 1% penicillin-streptomycin (Meiji Seika, Tokyo, Japan), 0.4 μg/mL hydrocortisone (saxizon; Kowa, Tokyo, Japan), 2 nM triiodo-thyronine (T3; Sigma Aldrich, Tokyo, Japan), 1 nM cholera toxin (List Biological Laboratories, Inc., Campbell, CA, USA), and 10 ng/mL EGF (Higeta Shoyu, Tokyo, Japan). Incubation was carried out at 37°C and 5% CO_2. All procedures were carried out following the formation of mature, stratified epithelial cell sheets.

Cell Culture: Human Limbal Epithelial Cell Sheets

Human corneas (donor age 34–73) were obtained from eye banks (Sightlife, Seattle, WA, USA) and subsequently washed in DMEM before being incubated in dispase for 1 hour at 37°C 5% CO_2. The human limbal keratinocytes (HLK) were then scraped from the limbal region of the cornea, and the resulting suspension was centrifuged and the supernatant removed. The cells then underwent trypsinization before being resuspended in KCM and seeded at an initial cell density of 1×10^5 cells/mL into 12-well culture inserts (Falcon) with MMC-treated 3T3-J2 feeder cells in KCM, separated by the cell culture insert permeable membrane. Incubation was carried out at 37°C and 5% CO_2. All procedures were carried out following the formation of mature, stratified epithelial cell sheets.

Quantum Dot Incubation and Analysis

Incubation media was formulated to either contain the standard 1.64 mM of calcium, or 0 mM of calcium with 5 mM of the calcium chelator EGTA. In order to standardize the level of tight junction disruption, EGTA was used to remove any tight junction–associated calcium, as well as any calcium remaining from the use of KCM medium during the culturing period. Green (525 nm) and red (655 nm) quantum dots, with zinc sulfide shells conjugated to carboxyl molecules, were purchased as a suspension in borate buffer (GIBCO Invitrogen Life Technologies). Forty nanometer suspensions of both green and red quantum dots were made by diluting the commercially available quantum dots into either the calcium or EGTA containing incubation media. The pH of all incubation media was then adjusted to 7.4, and then applied to the superficial surface of the epithelial cell sheets. These were then incubated at 37°C and 5% CO_2 for 90 minutes. The cell sheets were washed twice in PBS to remove any excess quantum dots. The samples were then immunostained with a 10% Hoechst solution for 10 minutes, following which they were fixed in 4% paraformaldehyde and analyzed using confocal microscopy (Ziess, Jena, Germany). Confocal parameters (including laser power, aperture size, and image thresholds) were identical for all samples.

Transepithelial Electrical Resistance (TEER)

Electrical resistance across the cell sheets was measured using an EndOhm chamber (WPI, Inc., Sarasota, FL, USA) and EVOM2 resistance meter (WPI, Inc.). An insert containing only medium, with no cell culture, was used as a blank.
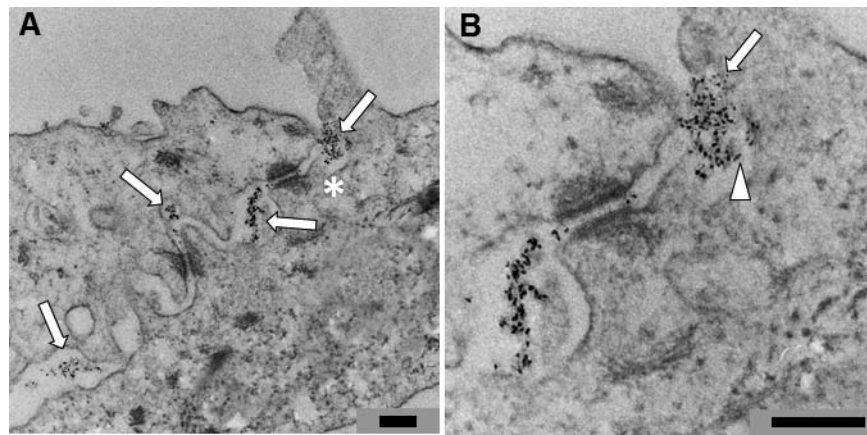
FIGURE 1. Transmission electron microscopy micrographs showing oral mucosal epithelial cells and the penetration of quantum dots into the paracellular space. (**A**) Taken at ×8000 magnification, several clusters of quantum dots can be seen residing in the paracellular space (*arrows*). The area marked by the asterisk can be seen at ×20,000 magnification in Figure 1B. In (**B**), small spherical green quantum dots are indicated by an *arrow*. While larger, more elongated red quantum dots are indicated by an *arrowhead. Scale bar*: 200 nm.

Transepithelial electrical resistance was measured at various time points after addition of the incubation media. The TEER value was first measured at 0 minutes after incubation, then every 15 minutes following for a period of 90 minutes. Each test was performed in triplicate for each condition. The TEER value was calculated by: [average resistance of experimental wells − average resistance of blank wells] Ohms × 0.33 cm^2 (area of the insert culture surface).

MTT Cell Viability Assay

Stock solution of MTT (Sigma Aldrich) was diluted to 375 μg/mL in KCM. A 5 mM EGTA solution and/or 40 nM suspensions of both green and red quantum dots were then added to this MTT-KCM medium. This was then pipetted into 12-well inserts containing HOK or HLK derived cell sheets. After incubation at 37°C for 2 hours, the resulting formazan crystals were dissolved in equal quantities of acidified isopropanol. The data was obtained by subtracting the background absorbance at 690 nm from the absorbance at 570 nm recorded using a spectrophotometer (V-550, UV/VIS Spectrophotometer; JASCO, Tokyo, Japan) and expressed as a percentage of the control cell sheets incubated without quantum dots or EGTA. Each test was performed in triplicate for each condition. ANOVA and Dunnett's statistical analysis was carried out using JMP software (JMP, Cary, NC, USA) to compare each test value with the control group.

Transmission Electron Microscopy (TEM)

Following incubation with the quantum dot suspensions, samples were fixed in a solution of 2.5% glutaraldehyde and 2% paraformaldehyde in 0.1 M sodium cacodylate buffer (pH 7.2) at room temperature for 3 hours. Staining was then carried out with 2% osmium tetraoxide for 1 hour followed by 0.5% uranyl acetate for 1 hour at room temperature. The samples were then dehydrated through graded alcohols and propylene oxide before being embedded in Araldite resin (TAAB Laboratories, Reading, UK). Resin curing was carried out at 60°C for 3 days. Ninety-nanometer thick sections were cut from the cured sample blocks on a Reichert-Nissei Ultracut Microtome (Leica, Wien, Austria) and floated onto copper mesh-200 EM grids (Agar Scientific Ltd., Stansted, UK). These were then post stained at room temperature in 2% aqueous uranyl acetate and Reynolds lead citrate for 5 minutes.

In order to measure the particle size, droplets of red and green quantum dots were also applied to the surface of carbon film coated slot-grids (Agar Scientific Ltd.). Any excess solution was wicked away using filter paper. All grids were then given time to dry before TEM examination.

Analysis of all samples was carried out at 80 kV with a transmission electron microscope (Hitachi, Tokyo, Japan). Images were obtained with a charge-coupled device camera (Gatan, Inc., Tokyo, Japan).

Quantum Dot Size Measurements

Micrographs were obtained of the quantum dots on carbon film coated slot-grids. Length and width values for both red and green quantum dots were calculated from 15 measurements taken using Fiji (ImageJ; http://imagej.nih.gov/ij/; provided in the public domain by the National Institutes of Health, Bethesda, MD, USA) software.

Fluorescence Intensity Measurements

Fluorescence intensity readings were taken across the *XY*-plane of the confocal micrographs at 1-μm interval passing through the thickness of the cell sheet. By calculating the area under the curve of the subsequent fluorescence intensity graph, total fluorescence intensity was determined. Mean total fluorescence intensity, peak fluorescence intensity, and depth of the peak fluorescence intensity within the cell sheet were calculated from reading from three sample cell sheets. *P* values were obtained via *t*-test statistical analysis.

RESULTS

The TEM micrographs in Figure 1 show small populations of quantum dots (Fig. 1A, arrows) residing within the paracellular space. The area marked by an asterisk can be seen at higher magnification in Figure 1B, where it is possible to discern the small green (arrow) and larger red (arrowhead) quantum dots.

The TEM micrograph Figure 2A1 shows the green quantum dots were approximately spherical in shape, with a mean width of 3.16 nm (SD = 0.30 nm) and a mean length of 3.28 nm (SD = 0.19 nm; Fig. 2A2). The red quantum dots (Fig. 2B1) had a more oblong shape, with a width of 5.54 nm (SD = 0.29 nm) and a length of 14.98 nm (SD = 1.02 nm; Fig. 2B2). For a full list of size measurements see Supplementary Table S1.
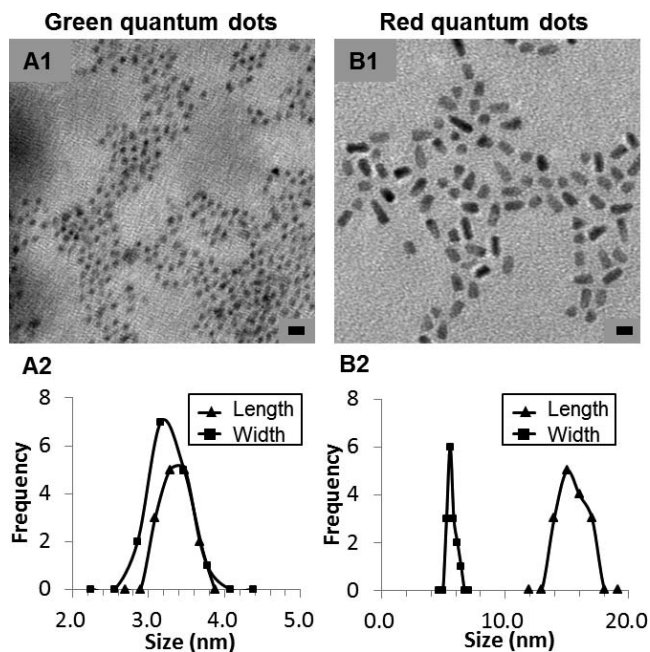
Green quantum dots

Red quantum dots

FIGURE 2. Transmission electron microscopy micrographs of quantum dots (**A1**, **B1**). *Scale bar*: 10 nm. (**A2**) and (**B2**) show frequency distribution of the quantum dot length and width measurements.

Figure 3 demonstrates the effect of incubating HOK and HLK cell sheets in 0 mM calcium medium with an EGTA calcium chelator. In 1.64 mM of calcium, the initial electrical resistance of the cell sheet was approximately maintained throughout the 90 minutes of incubation. However, using medium containing 0 mM of calcium with 5 mM of EGTA had the effect of rapidly reducing the cell sheet's electrical resistance within the first 15 minutes. A slowing, but continued decrease occurred for the following 75 minutes until after 90 minutes the resistance was significantly lower than its initial level, corresponding to an average 18.3 Ohms·cm^2 reduction in the HOK cell sheets, and a 22.8
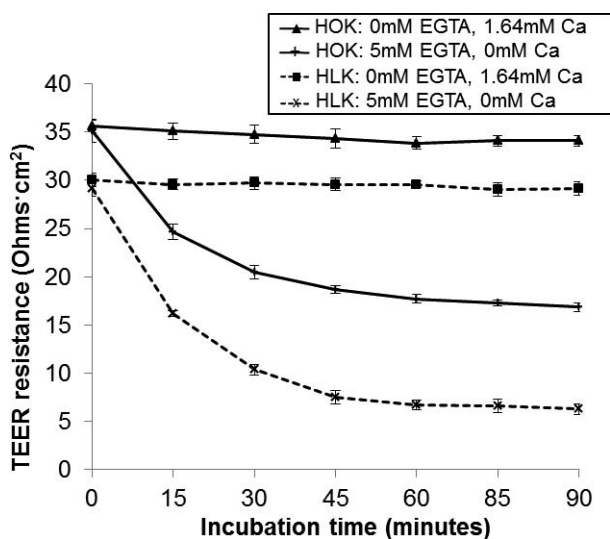

FIGURE 3. Graph showing the effect of low calcium on cell sheet TEER. Initial resistance levels are approximately maintained when the cell sheet is incubated in normal calcium levels of 1.64 mM. Using a calcium chelator (EGTA) in medium containing 0 mM of calcium resulted in a reduction in electrical resistance. *Error bars* show SD. $n = 3$.
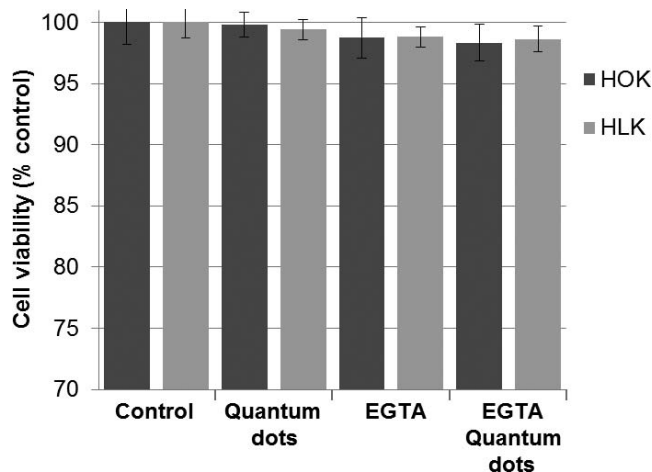

FIGURE 4. MTT cell viability assay. Following 2 hours incubation with 5 mM EGTA and/or green and red quantum dots, cell viability was not significantly reduced in any sample of cell sheets. *P* values for HOK when compared with the control: QD 0.99, EGTA 0.74, EGTA QD 0.58. *P* values for HLK when compared with the control: QD 0.89, EGTA 0.55, EGTA QD 0.44.

Ohms·cm^2 reduction in the HLK cell sheets. Figure 4 shows that incubation for 2 hours with EGTA and/or quantum dots had no significant effect of the viability of either the HOK- or HLK-derived cell sheets.

The confocal micrographs in Figures 5 show a significant difference in quantum dot quantity and distribution across the healthy HOK (Fig. 5A1) and HLK (Fig. 5B1) cell sheets compared with the cell sheets containing damaged tight junctions (HOK Fig. 5A2 and HLK Fig. 5B2). In the healthy cell sheets, small amounts of quantum dots can be seen residing on the surface and in the border regions between cells (Figs. 5A1, 5B1, arrowhead). The damaged cell sheets show significantly larger amount of quantum dots residing in the paracellular space, creating a much stronger fluorescence profile for both the red and green quantum dots (Figs. 5A2, 5B2, arrows).

Figure 6 shows the Z-plane surface (cross-section) rendered views through the HOK and HLK cell sheets of Figure 5. The same rendered view, with the addition of cell nuclei Hoechst staining, can be seen in Supplementary Figure S1. The healthy cell sheets (Figs. 6A, 6C) contain a thin layer of quantum dots residing on the surface (arrow). Both red and green quantum dots are present in this residual layer. The damaged cell sheets however, contain a superficial layer of quantum dots (Figs. 6B, 6D, arrowheads) over two times thicker than in the healthy cell sheets. In addition, numerous populations of green (and to a lesser extent, red) quantum dots can also be seen within the deeper cell layers. The asterisk in Figure 6B2 indicates a large cluster of green quantum dots residing in a deeper region. No such deeper populations can be observed in the healthy cell sheet.

Figure 7 shows the fluorescence intensity readings taken from the confocal micrographs in Figure 6. In the damaged cell sheets (Figs. 7A2, 7B2), the initial fluorescence peak is both stronger in intensity and continues deeper into the cell sheet than in the healthy cell sheets (Figs. 7A1, 7B1). Following this initial peak, green quantum dot fluorescence is still present at a lower intensity level throughout the thickness of the cell sheets. The second large fluorescence peak seen in Figure 7A2 represents the large cluster of green quantum dots residing approximately 40-μm deep into the cell sheet (Fig. 6B2, asterisk). In the Table, the mean fluorescence intensity
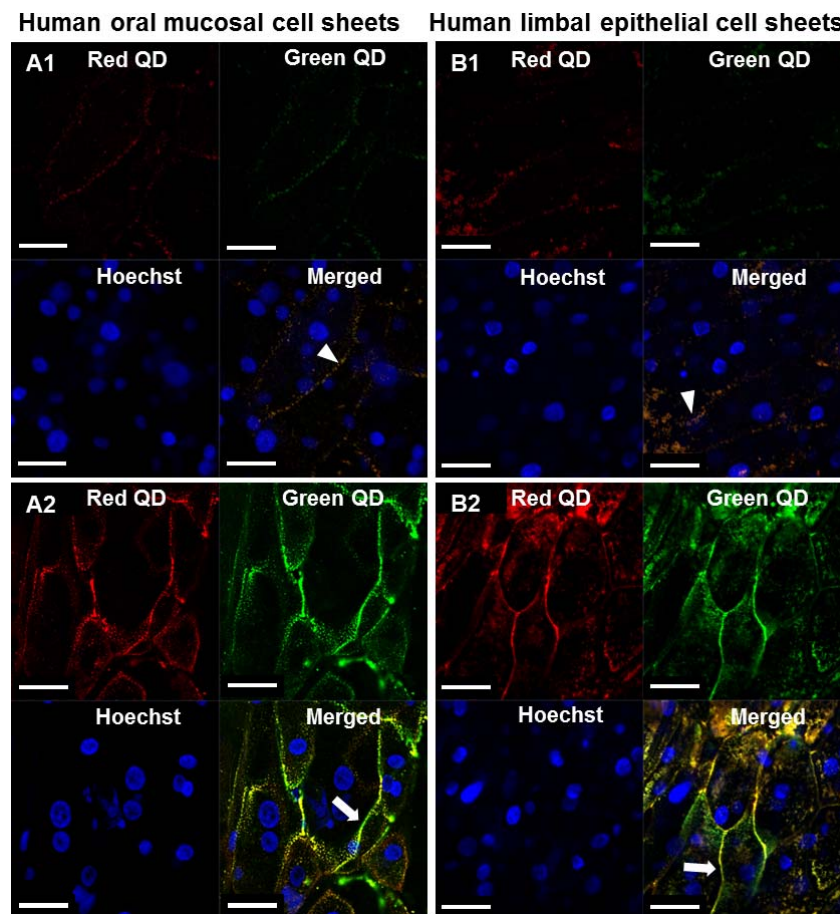
Human oral mucosal cell sheets

Human limbal epithelial cell sheets

FIGURE 5. *XY*-plane confocal micrographs of epithelial cell sheets incubated with green and red quantum dots. The healthy cell sheets (**A1**, **B1**) show low levels of quantum dot fluorescence on the surface and borders between cells (*arrowheads*). Stronger fluorescence can be seen in the cell sheets with damaged tight junctions (**A2**, **B2**). The *arrows* indicate areas where quantum dots are residing in the paracellular spaces. *Scale bars*: 50μm.

readings taken from multiple cell sheets show a statistically significant increase in both green (HOK $P = 0.038$, HLK $P = 0.009$) and red (HOK $P = 0.032$, HLK $P = 0.013$) quantum dot fluorescence intensity when comparing the healthy cell sheets to the damaged cell sheets. Furthermore, the peak intensity readings for the quantum dots occurred two to three times deeper into the damaged cell sheet than in the healthy cell sheets.

DISCUSSION

We have demonstrated that quantum dots can be used as an effective indicator of a cell sheet's barrier function. Our hypothesis can be confirmed as cell sheets with disrupted barrier function demonstrated deeper and more widespread penetration of the quantum dot nanoparticles, particularly of the smaller green quantum dots. By applying quantum dots in this way, nano and microscale morphologic information on a cell sheet's surface and interior can also be ascertained, in particular, making local areas of abnormality or increased permeability easy to identify, something that current evaluation techniques, such as TEER, are unable to provide.

Transepithelial electrical resistance did however demonstrate the dramatic effect caused by EGTA calcium chelation. This was in turn mirrored by the significant increase in quantum dot penetration through the open paracellular spaces, penetrating even through to the deepest layers of

the cell sheets. These results demonstrate that tight junctions are a major factor in a cell sheet's barrier function. However, even in the damaged cell sheets, the larger red quantum dots showed a more limited penetration deeper than 15 μm into the cell sheet. This parallels results from another quantum dot penetration studies, which recorded red (655 nm) quantum dots showing limited penetration deeper than 15 to 20 μm into the epithelium of an intact cornea after a similar 80 minutes incubation in vivo.[39] This suggests that the size of the quantum dot was a limiting factor for its penetration through the cell sheet. A model for the observed penetration of the quantum dots can be seen in Figure 8. Other junctional complexes such as adherens junctions, desmosomes, and gap junctions serve to anchor or connect neighboring epithelial cells together. It has previously been reported that the paracellular space adjacent to adherens junctions and desmosomes is approximately 20 to 30 nm.[40-43] However, the presence of gap junctions reduces this space to 4 nm.[41,43] The red quantum dots, with a recorded length of 14.98 nm and a width of 5.54 nm, would be too large to pass through these narrow paracellular regions containing gap junctions. Consequently, even though the damaged cell sheet had disrupted tight junctions, the gap junctions may still have served to slow the rate of passage of the red quantum dots through to the deeper regions of the cell sheet.

Conversely, the green quantum dots, with a recorded length of 3.28 nm and a width of 3.16 nm, would be small enough to pass through even the narrowest regions in the paracellular
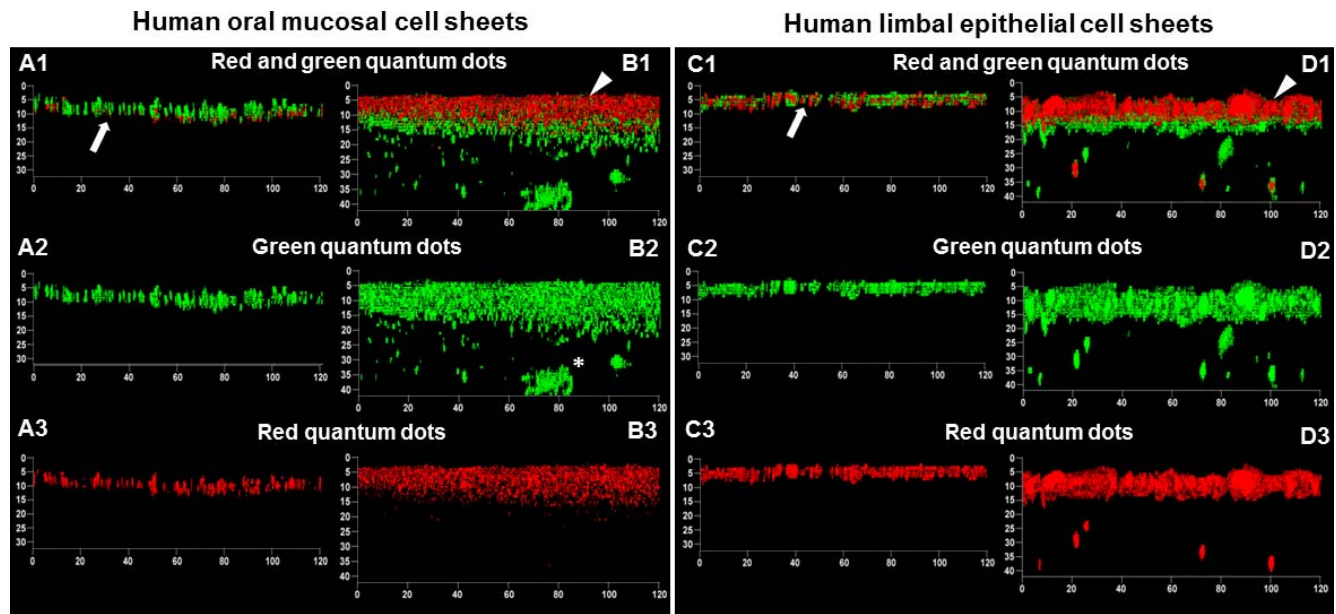
FIGURE 6. *Z*-plane (cross-section) surface-rendered confocal micrographs of epithelial cell sheets incubated with green and red quantum dots. The healthy cell sheets (**A**, **C**) show a thin layer of quantum dot fluorescence in the superficial most area (*arrow*). The damaged cell sheets (**B**, **D**) show a thick layer of strong fluorescence in the superficial area (*arrowheads*) and deeper populations of green quantum dot fluorescence (*asterisk*). All scales are measured in micrometers.

space. Although the rate at which they could pass through these regions would still be rate limited and time dependant. This may explain why although deeper populations of green quantum dots were observed in the damaged cell sheet, a large proportion of them remained in the more superficial layers. Nevertheless, a relatively large quantity of the quantum dots (labelled by an asterisk in Fig. 6B2) were able to accumulated at the bottom of the cell sheet in such a localized manner as to suggest particular disruption or damage to that area of the cell sheet. In this way, quantum dots can be used to identity localized areas of abnormality within the cell sheet.

As green (to a lesser extent, red) quantum dots were able to penetrate deeply into the cell sheet, we also investigated whether penetration rates could be quantifiably measured by analyzing the medium collected from beneath the cell sheets
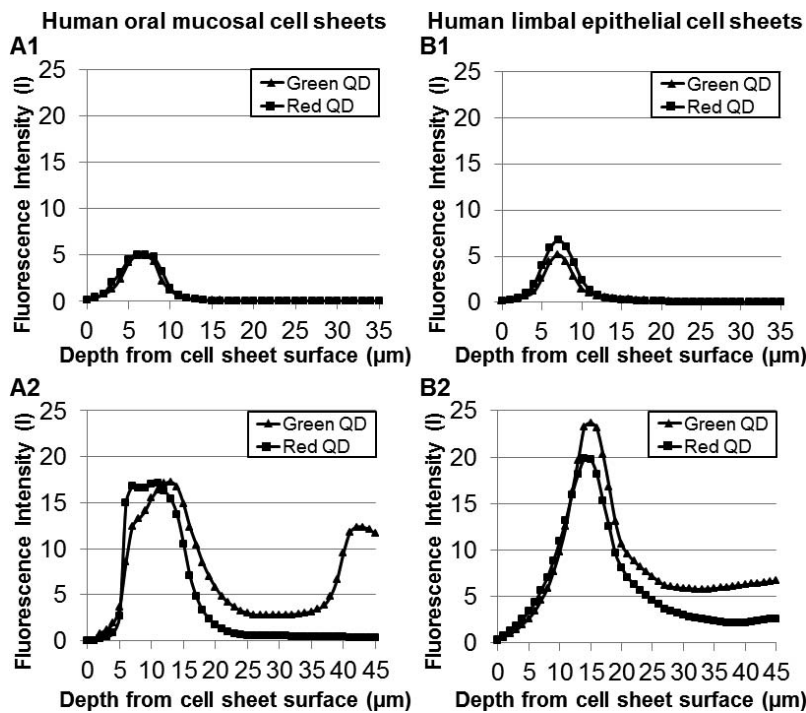

FIGURE 7. Fluorescence intensity graphs from epithelial cell sheets incubated with green and red quantum dots. Fluorescence intensity in the healthy (**A1**, **B1**) and damaged (**A2**, **B2**) cell sheets was measured using data from the confocal micrographs in Figure 6. These intensity graphs show quantum dot fluorescence as a function of depth through the cell sheet.

TABLE. Mean Cell Sheet Fluorescence Intensity Data

| | Human Oral Mucosal Cells | | | | Human Limbal Epithelial Cells | | | |
| | Healthy Cell Sheets | | Damaged Cell Sheets | | Healthy Cell Sheets | | Damaged Cell Sheets | |
	Red QD	Green QD	Red QD	Green QD	Red QD	Green QD	Red QD	Green QD
Mean total fluorescence intensity, I	36.99 ± 9.02	38.09 ± 5.60	246.74 ± 69.20	416.15 ± 134.26	40.28 ± 5.54	31.82 ± 4.59	279.57 ± 49.17	403.00 ± 62.53
Mean peak fluorescence intensity, I	5.65 ± 0.57	5.33 ± 0.50	18.2 ± 1.56	18.34 ± 3.01	6.40 ± 1.08	5.38 ± 0.87	16.91 ± 2.66	20.43 ± 4.13
Mean depth of peak intensity, μm	6.00 ± 1.00	6.33 ± 1.53	12.33 ± 2.31	13.00 ± 1.00	6.00 ± 1.73	6.33 ± 2.08	18.33 ± 4.04	19.00 ± 4.00

A significant increase in total quantum dot fluorescence occurs in the damaged cell sheets compared with the healthy cell sheets. The peak intensity was also stronger and occurred deeper in the damaged cell sheets. $n = 3$. When comparing damaged cell sheet data with healthy cell sheet data, all $P < 0.038$.
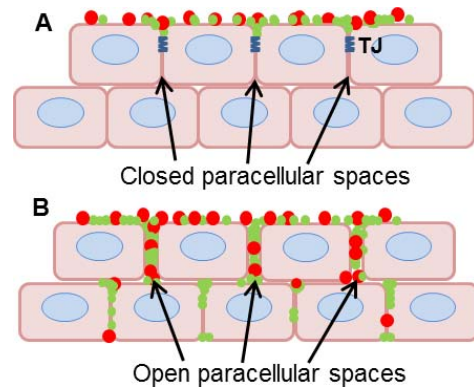

FIGURE 8. The quantum dot penetration model (A, B). Cell sheets with damaged or disrupted tight junctions have opened paracellular pathways resulting in greater quantum dot penetration in the superficial layers.

after incubation. The results of this experiment can be seen in the Supplementary Figure S2 and Supplementary Table S2.

Conventional methods for evaluating epithelial barrier function or surface abnormalities include measuring TEER or using fluorescent dyes such as sodium fluorescein. While these techniques are useful, our novel method can provide rapid nano and microscale structural information on a cell sheet's surface and interior morphology as well as the health of its barrier function, allowing localized areas of surface abnormality or damage to be easily identified. Standard fluorescent dye molecules may be small enough (sodium fluorescein radius = 5.5 Å[44]) to pass through the paracellular space rapidly and with ease. Quantum dots are considerably larger than these dye molecules; accordingly they may show a comparably slower rate of penetration through the cell sheet. The quantum dots often aggregated into small clusters as they moved through the paracellular space into the deeper cell layers, with larger aggregations occurring in areas of increased permeability. Subsequently, quantum dots can provide structural information on the interior morphology of a cell sheet on a nano and microscale, ranging from as small as 3.16 nm (the width of a single green quantum dot) up to the large aggregation that often measure 5 to 10 μm in size. This is something that the smaller dye molecules are unable to provide.

However, further improvements to this technique can be made. There are discrepancies in the current literature regarding the toxicity of quantum dots. This is largely due to the variety of quantum dots available, and a lack of extensive toxicity studies. Our own investigations align with longer term studies that show no appreciable toxicity.[45–47] Conversely, some studies have reported that despite the zinc sulfide shell, Cd^{2+} ions are able to leech out of the quantum dot core, causing concerns about their toxicity and safety for clinical use.[48] Furthermore, comparative confocal micrographs in Supplementary Figure S3 show that even in unfixed cell sheets, the quantum dots are not readily removed from the paracellular spaces once they have penetrated the cell sheet. Even so, this technique could still be applied to cell sheets in vitro, together with other destructive tests such as immunohistochemistry.[21] A range of in vivo application are currently being considered using alternatives, such as carbon quantum dots[49] or indium phosphide[50,51] that have been shown to possess significantly lower levels of cytotoxicity.

In addition, using a greater range of quantum dot sizes would potentially produce a spectrum of color across the thickness of the cell sheet, giving more information on the degree to which the paracellular pathway is open. It may be

possible to define the scale of tight junction disruption by observing the relative penetration of different sized quantum dots. Based on our experiments, the smallest quantum dots would be expected to penetrate to the deepest layers. Small or intermediate sized quantum dots may penetrate the superficial layers but at a reduced rate, while the larger quantum dots would remain on the surface or in the most superficial layer. This data would then provide greater information on a cell sheet's barrier function as well as local areas of abnormality.

For this proof-of-concept study, using EGTA to disrupt tight junction function was desirable as it induced a significant effect on TEER. However, future work will feature a range of disruptive techniques, in order to better represent the variety of abnormalities and defects common in cultured cell sheets. One such candidate for future study as an alternative and milder disruptor of tight junction function is TNF–α. This was tested following published protocols,[52-54] briefly, the cell sheets were incubated for 24 hours with 10 ng/mL TNF–α, before the addition of red and green quantum dots. Transepithelial electrical resistance readings and comparative confocal micrographs can be seen in Supplementary Figure S4.

To conclude, our method for evaluating cultured epithelial cell sheet barrier function has not been reported in the literature to date. As such, it represents a novel technique to provide clear, easy to interpret data on a cell sheet's barrier function, as well as nano and microscale structural information of its interior and surface morphology. This technique can be incorporated into the range of analytical tests performed prior to approval for transplantation. Furthermore, this information may serve to enhance scientific knowledge on how to fabricate healthy cell sheets for transplantation.

Acknowledgments

Disclosure: **T.J. Duncan**, None; **K. Baba**, None; **Y. Oie**, None; **K. Nishida**, None

References

1. Schermer A, Galvin S, Sun TT. Differentiation-related expression of a major 64K corneal keratin in vivo and in culture suggests limbal location of corneal epithelial stem cells. *J Cell Biol*. 1986;103:49–62.

2. Cotsarelis G, Cheng S-Z, Dong G, Sun TT, Lavker RM. Existence of slow-cycling limbal epithelial basal cells that can be preferentially stimulated to proliferate: implications on epithelial stem cells. *Cell*. 1989;57:201–209.

3. Shapiro M, Friend J, Thoft R. Corneal re-epithelialization from the conjunctiva. *Invest Ophthalmol Vis Sci*. 1981;21:135–142.

4. Dua H, Forrester J. The corneoscleral limbus in human corneal epithelial wound healing. *Am J Ophthalmol*. 1990;110:646–656.

5. Tsubota K, Satake Y, Kaido M, et al. Treatment of severe ocular-surface disorders with corneal epithelial stem-cell transplantation. *N Engl J Med*. 1999;340:1697–1703.

6. Pellegrini G, Traverso CE, Franzi AT, et al. Long-term restoration of damaged corneal surfaces with autologous cultivated corneal epithelium. *Lancet*. 1997;349:990–993.

7. Nishida K, Yamato M, Hayashida Y, et al. Functional bioengineered corneal epithelial sheet grafts from corneal stem cells expanded ex vivo on a temperature-responsive cell culture surface. *Transplantation*. 2004a;77:379–385.

8. Nakamura T, Inatomi T, Sotozono C, Koizumi N, Kinoshita S. Successful primary culture and autologous transplantation of corneal limbal epithelial cells from minimal biopsy for unilateral severe ocular surface disease. *Acta Ophthalmol (Scand)*. 2004a;82:468–471.

9. Chen J, Tseng S. Corneal epithelial wound healing in partial limbal deficiency. *Invest Ophthalmol Vis Sci*. 1990;31:1301–1314.

10. Dua HS, Azuara-Blanco A. Autologous limbal transplantation in patients with unilateral corneal stem cell deficiency. *Br J Ophthalmol*. 2000;84:273–278.

11. Kwitko S, Marinho D, Barcaro S, et al. Allograft conjunctival transplantation for bilateral ocular surface disorders. *Ophthalmology*. 1995;102:1020–1025.

12. Samson CM, Nduaguba C, Baltatzis S, Foster CS. Limbal stem cell transplantation in chronic inflammatory eye disease. *Ophthalmology*. 2002;109:862–868.

13. Rao SK, Rajagopal R, Sitalakshmi G, Padmanabhan P. Limbal allografting from related live donors for corneal surface reconstruction. *Ophthalmology*. 1999;106:822–828.

14. Daya SM. Living related conjunctival limbal allograft for the treatment of stem cell deficiency. *Ophthalmology*. 2001;108:126–133.

15. O'Connor N, Mulliken J, Banks-Schlegel S, Kehinde O, Green H. Grafting of burns with cultured epithelium prepared from autologous epidermal cells. *Lancet*. 1981;317:75–78.

16. Madhira SL, Vemuganti G, Bhaduri A, Gaddipati S, Sangwan VS, Ghanekar Y. Culture and characterization of oral mucosal epithelial cells on human amniotic membrane for ocular surface reconstruction. *Mol Vis*. 2008;14:189.

17. Nakamura T, Endo K-I, Cooper LJ, et al. The successful culture and autologous transplantation of rabbit oral mucosal epithelial cells on amniotic membrane. *Invest Ophthalmol Vis Sci*. 2003;44:106–116.

18. Hayashida Y, Nishida K, Yamato M, et al. Ocular surface reconstruction using autologous rabbit oral mucosal epithelial sheets fabricated ex vivo on a temperature-responsive culture surface. *Invest Ophthalmol Vis Sci*. 2005;46:1632–1639.

19. Nishida K, Yamato M, Hayashida Y, et al. Corneal reconstruction with tissue-engineered cell sheets composed of autologous oral mucosal epithelium. *N Engl J Med*. 2004b;351:1187–1196.

20. Nakamura T, Inatomi T, Sotozono C, Amemiya T, Kanamura N, Kinoshita S. Transplantation of cultivated autologous oral mucosal epithelial cells in patients with severe ocular surface disorders. *Br J Ophthalmol*. 2004b;88:1280–1284.

21. Hayashi R, Yamato M, Takayanagi H, et al. Validation system of tissue-engineered epithelial cell sheets for corneal regenerative medicine. *Tissue Eng Part C Methods*. 2009;16:553–560.

22. Surgrue SP, Zieske JD. ZO1 in corneal epithelium: association to the zonula occludens and adherens junctions. *Exp Eye Res*. 1997;64:11–20.

23. Yap A, Mullin J, Stevenson B. Molecular analyses of tight junction physiology: insights and paradoxes. *J Membr Biol*. 1998;163:159–167.

24. Meldolesi J, Castiglioni G, Parma R, Nassivera N, De Camilli P. Ca++-dependent disassembly and reassembly of occluding junctions in guinea pig pancreatic acinar cells. Effect of drugs. *J Cell Biol*. 1978;79:156–172.

25. Siliciano J, Goodenough DA. Localization of the tight junction protein, ZO-1, is modulated by extracellular calcium and cell-cell contact in Madin-Darby canine kidney epithelial cells. *J Cell Biol*. 1988;107:2389–2399.

26. Gonzalez-Mariscal L, Contreras R, Bolivar J, Ponce A, Chavez De Ramirez B, Cereijido M. Role of calcium in tight junction formation between epithelial cells. *Am J Physiol*. 1990;259(6 pt 1):978–986.

27. Contreras R, Miller J, Zamora M, Gonzalez-Mariscal L, Cereijido M. Interaction of calcium with plasma membrane of epithelial

Investigative Ophthalmology & Visual Science

(MDCK) cells during junction formation. *Am J Physiol*. 1992; 263(2 pt 1):C313–C318.

28. Martinez-Palomo A, Meza I, Beaty G, Cereijido M. Experimental modulation of occluding junctions in a cultured transporting epithelium. *J Cell Biol*. 1980;87:736–745.

29. Stevenson BR, Anderson JM, Goodenough DA, Mooseker MS. Tight junction structure and ZO-1 content are identical in two strains of Madin-Darby canine kidney cells which differ in transepithelial resistance. *J Cell Biol*. 1988;107:2401–2408.

30. Balda MS, Whitney JA, Flores C, González S, Cereijido M, Matter K. Functional dissociation of paracellular permeability and transepithelial electrical resistance and disruption of the apical-basolateral intramembrane diffusion barrier by expression of a mutant tight junction membrane protein. *J Cell Biol*. 1996;134:1031–1049.

31. Blume LF, Denker M, Gieseler F, Kunze T. Temperature corrected transepithelial electrical resistance (TEER) measurement to quantify rapid changes in paracellular permeability. *Pharmazie*. 2010;65:19–24.

32. Butor C, Davoust J. Apical to basolateral surface area ratio and polarity of MDCK cells grown on different supports. *Exp Cell Res*. 1992;203:115–127.

33. Lo C-M, Keese CR, Giaever I. Cell–substrate contact: another factor may influence transepithelial electrical resistance of cell layers cultured on permeable filters. *Exp Cell Res*. 1999;250: 576–580.

34. Dabbousi B, Rodriguez-Viejo J, Mikulec FV, et al. (CdSe) ZnS core-shell quantum dots: synthesis and characterization of a size series of highly luminescent nanocrystallites. *J Phys Chem B*. 1997;101:9463–9475.

35. Leatherdale C, Woo W-K, Mikulec F, Bawendi M. On the absorption cross section of CdSe nanocrystal quantum dots. *J Phys Chem B*. 2002;106:7619–7622.

36. Murphy CJ. Peer reviewed: optical sensing with quantum dots. *Analytical Chem*. 2002;74:520, A-6 A.

37. Alivisatos P. The use of nanocrystals in biological detection. *Nat Biotechnol*. 2003;22:47–52.

38. Parak WJ, Gerion D, Pellegrino T, et al. Biological applications of colloidal nanocrystals. *Nanotechnology*. 2003;14:R15.

39. Kuo TR, Lee CF, Lin SJ, et al. Studies of intracorneal distribution and cytotoxicity of quantum dots: risk assessment of eye exposure. *Chem Res Toxicol*. 2011;24:253–261.

40. Ozanics V, Rayborn M, Sagun D. Some aspects of corneal and scleral differentiation in the primate. *Exp Eye Res*. 1976;22: 305–327.

41. Mishima S. Clinical investigations on the corneal endothelium. *Ophthalmology*. 1982;89:525–530.

42. He W, Cowin P, Stokes DL. Untangling desmosomal knots with electron tomography. *Science*. 2003;302:109–113.

43. Maeda S, Nakagawa S, Suga M, et al. Structure of the connexin 26 gap junction channel at 3.5 Å resolution. *Nature*. 2009;458: 597–602.

44. Jampol L, Cunha-Vaz J. Diagnostic agents in ophthalmology: sodium fluorescein and other dyes. Pharmacology of the eye. In: Sears ML, ed. *Handbook of Experimental Pharmacology*. Vol. 69. Berlin, Heidelberg: Springer; 1984:699–714.

45. Voura EB, Jaiswal JK, Mattoussi H, Simon SM. Tracking metastatic tumor cell extravasation with quantum dot nanocrystals and fluorescence emission-scanning microscopy. *Nat Med*. 2004;10:993–998.

46. Hoshino A, Hanaki K, Suzuki K, Yamamoto K. Applications of T-lymphoma labeled with fluorescent quantum dots to cell tracing markers in mouse body. *Biochem Biophys Res Commun*. 2004;314:46–53.

47. Hauck TS, Anderson RE, Fischer HC, Newbigging S, Chan WC. In vivo quantum-dot toxicity assessment. *Small*. 2010;6:138–144.

48. Hardman, R. A toxicologic review of quantum dots: toxicity depends on physicochemical and environmental factors. *Environ Health Perspect*. 2006;165–172.

49. Yang ST, Cao L, Luo PG, et al. Carbon dots for optical imaging in vivo. *J Am Chem Soc*. 2009;131:11308–11309.

50. Brunetti V, Chibli H, Fiammengo R, et al. InP/ZnS as a safer alternative to CdSe/ZnS core/shell quantum dots: in vitro and in vivo toxicity assessment. *Nanoscale*. 2013;5:307–317.

51. Mushonga P, Onani MO, Madiehe AM, Meyer M. Indium phosphide-based semiconductor nanocrystals and their applications. *J Nanomaterials*. 2012;2012:12.

52. Schmitz H, Fromm M, Bentzel CJ, et al. Tumor necrosis factor-alpha (TNFalpha) regulates the epithelial barrier in the human intestinal cell line HT-29/B6. *J Cell Sci*. 1999;112:137–146.

53. Ma TY, Iwamoto GK, Hoa NT, et al. TNF-α-induced increase in intestinal epithelial tight junction permeability requires NF-κB activation. *Am J Physiol Gastrointest Liver Physiol*. 2004;286: G367–G376.

54. Ma TY, Boivin, MA, Ye D, Pedram A, Said HM. Mechanism of TNF-α modulation of Caco-2 intestinal epithelial tight junction barrier: role of myosin light-chain kinase protein expression. *Am J Physiol Gastrointest Liver Physiol*. 2005;288:G422–G430.